Vol 10 Suppl., July 2001
1009-1963/2001/10(Suppl.)/S195-11
Chinese Physics
© 2001 Chin. Phys. Soc.
and IOP Publishing Ltd

SETUP AND APPLICATION OF SCANNING NEAR-FIELD OPTICAL MICROSCOPY

Xu Shi-fa(许世发)[a], Zhu Xing(朱 星)[a], Zhou He-tian(周赫田)[a],
Shen Yu-min(沈玉民)[a], Fei Teng(费 滕)[a], Zhang Yu(张 宇)[a],
Yin Yan(尹 彦)[a], Zhang Bei(张 蓓)[a], Dai Lun(戴 伦)[a],
Liu Xiao-ling(刘晓玲)[b], Hu Jian-cheng(胡建成)[b],
Lu Ping(卢 萍)[b], and Zhai Zhong-he(翟中和)[b]

[a] *State Key Laboratory for Mesoscopic Physics and Department of Physics, Peking University, Beijing* 100871, *China*

[b] *College of Life Sciences Peking University, Beijing* 100871, *China*

(Received 28 March 2001)

The research on the setup and application of scanning near-field optical microscopy (SNOM) performed in our laboratory is reviewed in this report. We have constructed a versatile low temperature scanning near-field optical microscope with the capability of near-field imaging and spectroscopy, operating at liquid nitrogen temperature. A special designed coaxial double lens was used to introduce the illumination beam through a 200μm fiber; the detected optical signal was transmitted via a fiber tip to an avalanche photon detector. The performance test shows the stability of the new design. The shear force image and optical image of a standard sample are shown. A system of SNOM working at room temperature and atmosphere was used to characterize semiconductors and bio-molecular samples. It revealed the unique features of semiconductor microdisks in the near-field that is significantly different from that of far-field. The effects of different geographic microstructures on the near-field light distribution of InGaP, GaN, and InGaN multi-quantum-well microdisk were observed.

Keywords: near-field optics, scanning near-field optical microscope, microdisk, HeLa cells
PACC: 0779

I. INTRODUCTION

Scanning near-field optical microscope (SNOM) combines the spectroscopic and temporal selectivity of classical optical microscopy with a lateral resolution reaching well into the subwavelength regime beyond the diffraction limit of light, allowing to characterize, generate, and manipulate structures and dynamic properties of physics and chemistry, materials and biology.[1−3] Though the room-temperature SNOM working at ambient environment shows the ability of imaging subwavelength objects of semiconductors, nano-materials, materials for high density data storage etc., instrumentation working at low-temperature SNOM is highly demanded. As an important extension of SNOM, a low-temperature system has some obvious advantages: 1) the quantum efficiency of solids is increased dramatically as nonradiative processes are suppressed and radiative processes are enhanced at low temperatures, 2) the linewidth of an optical emission is generally much narrower at low temperatures, increasing the spectroscopic detail, and 3) the thermal noise of emission spectrum can be reduced drastically. Because of the above reasons, some groups have done a lot of work about quantum structures by using low-temperature SNOM systems.

In this report, we show a new design of low-temperature scanning near-field optical microscope (LT-SNOM). The compact system can be fed into a Dewar without low-temperature optical windows and no mechanical feed control. The illumination light and collected near-field optical signal are transmitted though two optical fibers.

The application of SNOM operated at ambient condition for characterizing semiconductors will be presented, i.e. the near-field optical properties of InGaP, GaN, and InGaN multi-quantum-well microdisk with different microstructures detected by using a SNOM.

Near-field optical features of bio-molecular (HeLa cells) will be shown.

II. INSTRUMENTATION OF OUR LOW TEMPERATURE SNOM[4]

A. Experimental Setup

The whole system consists of a cryostat, a scan-

ning head (Fig.1), an optical system, the scanning electronics and the image processing software. The scanning head is the primary part of the instrument, which consists of three basic components:

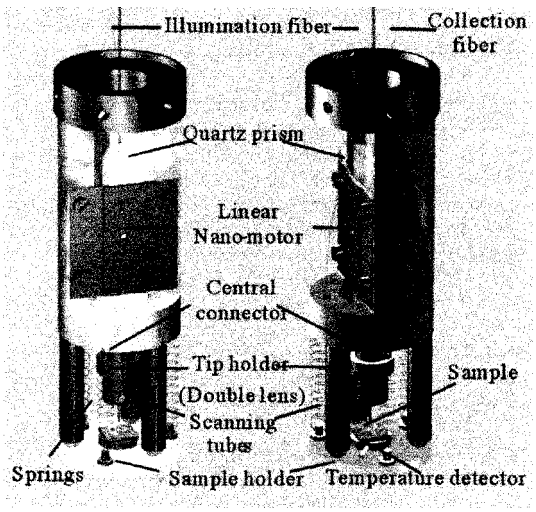


Fig.1. The scanning head. Left, the normal view, Right: the side view.

(a) A scanner unit to scan the sample holder;

(b) A central connector and tip holder which accomplish the shear force feedback control, and a small coaxial double lens optics;

1. The cryostat

The microscope is designed as an insert for a liquid nitrogen (LN) bathed cryostat, which consists of two glass Dewars, one of which is inserted into another, both of them are filled with LN. The scanning head is mounted in a stainless steel chamber, suspended by four springs from the top of the chamber. The chamber is immersed in LN and the interior is filled with nitrogen gas in order to provide good thermal exchange with the scanning head. Before cooling, the chamber was evacuated for dehumidification. No optical windows are made on the chamber, so that the mechanical and thermal stability can be improved. In this construction, the sample can be cooled down to 77.8K, within about 2h.

2. The scanning head

(i) The scanner unit The scanner unit (Fig.2) consists of three parallel piezotubes (PZT 5H, ϕ6.0mm×25mm, 0.5mm wall thickness), which are mounted equally spaced on a centreed 25mm diameter circle. The outer electrodes of these piezotubes are fourfold segmented for the x/y scanning. These segments of all three tubes are aligned in parallel. Upon driving the three piezotubes simultaneously, they behave like a single-tube scanner. The driving voltages addressed the segments of the three tubes are up to $\pm$200V, resulting in a maximum scan range of 10μm at room temperature. The driving voltages addressed inner electrodes range from 0 to 200V and result in a vertical movement 2μm at 300K. Because of the decrease of the piezoelectric constant at low temperatures, the maximum scan range and the vertical movement range reduce remarkably. The polishing sample holder is made of zirconia and connected to the scan tubes via three ruby balls and is clamped into place by three springs.

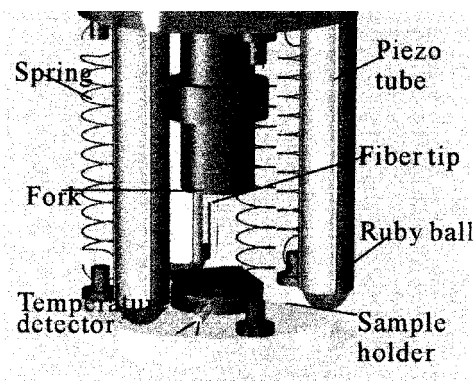


Fig.2. The scanner unit.

(ii) Feedback As in all scanning probe techniques, it is essential to be able to maintain the probe in a fixed distance above the surface. In our system, we use shear-force technique to control the tip-sample distance.[5] This technique is based on the measurement of the a mplitude of the current of a vibrating quartz fork, a fiber tip being glued on one hand. The fork is operated close to its resonance frequency (about 33kHz), and the damping is detected using a lock-in amplifier (Stanford SR830) by measuring the dissipated power. As the tip approaches to the sample, the vibration of the fork is damped by the shear force localized near the surface, and at the same time, the resonance frequency is shifted. The vibration signal measured by the lock-in amplifier (Stanford SR830) will decrease obviously, thus providing a reliable input parameter for the feedback operation. Input into the SPM controller (home-built control electronics) using a PI (Proportion and Integral) feedback, this signal generates the Z driving voltage, which makes the tip follow the sinuosity of the sample surface and presents a topography image. This feedback mode is a non-optical technique, no detecting optical beam is leaded

, so it is particularly suitable for the spectroscopic analysis.

(iii) The Linear nano-motor The motor's moving part is a quartz prism, which is clamped in-between six stacks of shear mode piezoelectrics, always two of them being located on each of the three side faces of the prism. The clamping force can be varied by adjusting the four screws. By addressing these shear piezoelectrics with a "saw-tooth" type of driving voltage (up to 300V, repetition at 50Hz), the quartz prism is moved by a "stick and slip" mode of motion. This piezoelectric stepping motor allows the controlled tip-sample coarse approach with a single step width between 30 and 150nm, and a maximum of moving range about 10mm. The Linear Nano-motor can be used in the environment of low temperature, ultra high vacuum and magnetic field. The motor is constructed after the design of Dr.S. H. Pan.

3. Optical system

In order to reduce the system's cost and to facilitate the adjustment of optical system, we use two fibers to input the exciting ray and export the near-field optical signal without any optical window on the cryogenic chamber. In the chamber, we accomplish the reflection and collection mode using a build-in coaxial two-lens optics (Fig.3).[6] The exciting ray is transmitted through the bottom of a 300μm illumination fiber, then is focused on a broad area of the sample under the tip by the two-lens (diameter 6mm, focal length 8.94mm). The fiber tip held in a hole of the double lens collects the near-field optical signal of the sample surface. We use a He-Ne laser as the emitter. The laser ray passes a mechanism chopper (EG&G 9479) and coupled into the illumination fiber by a lens. The near-field light is input in a Photo Multiplier Tube (PMT) and transferred to the electric voltage signal, which is detected by a Lock-in Amplifier (EG&G 5302) with the frequency signal of the chopper as a synchronous signal. The use of the chopper working at 1.00kHz increases the signal to noise ratio.

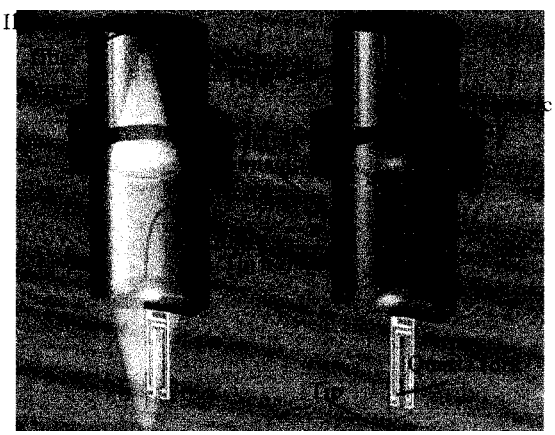


Fig.3. A build-in two-lens optical system.

4. Scanning electronics and image inquiring

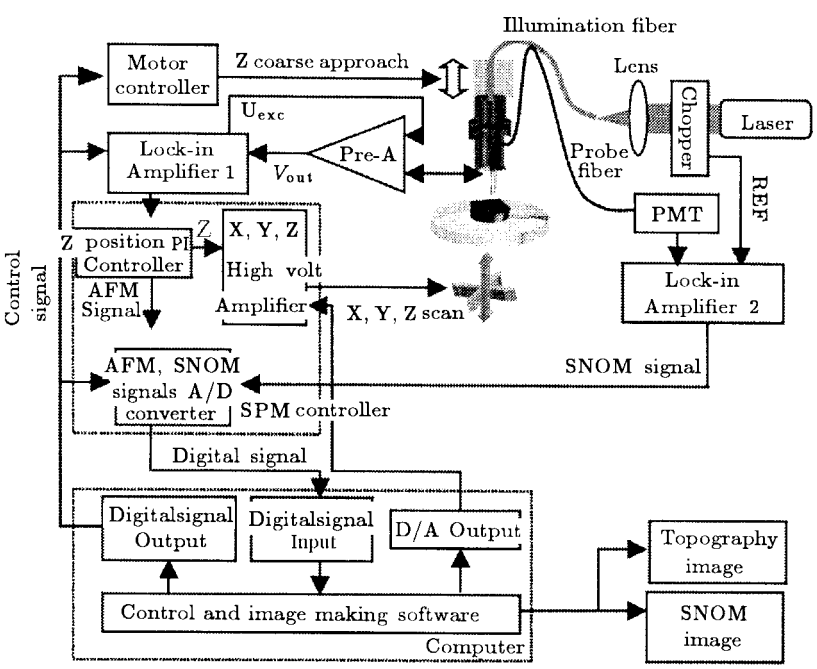


Fig.4. A schematic of the LT-SNOM system

A schematic graph of the whole system is showed in Fig.4. We use home-built scan electronics-SPM controller to generate images. This controller is used for x, y scan and tip-sample distance control. It includes an X, Y, Z high voltage amplifier, a Z position PI controller, an Analog/Digital (A/D) converter and the power supply. The analogous signals of the topography and the near-field optical graph are converted to digital signals by the A/D converter with the timesharing mode. The motor controller can drive the stepper motor to move by single step or continuously. The computer accomplishes the control of the whole system and the image processing. The X, Y scanning signal, which is generated by a 12-bit D/A board in the computer, is amplified by the SPM controller, then addresses the scanner unit.

B. Experimental results

The performance test shows the stability of the new design. The resolution of shear force imaging and optical image of standard sample are shown. There're some of the first images generated by our. The sample is the standard sample of grating from DI (Digital Instrument) Co. It is a gold film on the Si substrate and has $1\mu m \times 1\mu m$ square lattice, which consists of orthogonal convex lines (about 25nm in height) on the surface of the sample. The images in Fig.5 were obtained at room temperature. And the test at low temperature has been performed and the total system showed acceptable behavior. The primary images (not shown here) at LN-temperature indicate that the total design of the LT-SNOM has bee successful, but the detailed components need to refine.

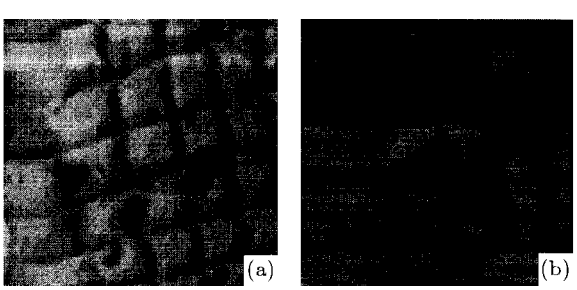


Fig.5. The images of the standard sample.(a)The topography of the sample,(b) The near-field optical image of the sample

Ⅲ. THE NEAR-FIELD OPTICAL PROPERTIES OF MULTI-QUANTUM-WELL MICRODISKS[7]

Optical microdisk is one of the typical micro cavities with disk-like shape resonant cavity. Because of the strong optical confinement to the gain region, high spontaneous emission coefficient and high quality factor can be achieved in microdisks.[8]

Unlike the conventional Fabry-Perot resonant cavity, the optical microdisk is characterized by a dominating optical whispering-gallery mode (WGM) light emission in which the optical wave travels around the circumference of the disk by total internal reflection and eventually gives rise to a narrow photon flux concentrated around the disk edge.[9] However, microdisk lasers with WGM mode have the problems of low power output and uncontrollable directionality. In order to improve the resonator properties, it is important to study the emission patterns of the disks by characterizing the light distribution of the photoluminescence (PL). Conventional PL spectroscopy and far-field fluorescence imaging have been applied to characterize the optical properties of microdisks. However, due to the diffraction limit of the light, the resolution of far field observation can not be better than half of the wavelength by conventional optical imaging method. We have constructed a combined system of near-field imaging (SNOM), near-field fluorescence and near-field spectroscopy, in conjunction with an optical microscopy.[10,11] With this system, we are able to map the local light distribution of the microdisks in nanometer scale. Here, we will present our results of the synthesis, optical characterization, and mode study by using SNOM technique of several types of semiconductor microdisks.

By using liquid phase epitaxy (LPE) or MOVPD and subsequent micro-processing procedures, we have synthesized four types semiconductor microdisks in two systems, InGaP, InGaAlP deformed microdisks on (100) n^+-GaAs substrate and GaN, InGaN multi-quantum-well microdisk with e-beam resist microstructure on the sapphire substrate. The diameters of the disks are ranging from 5 to 20 micros. The local light distribution of the microdisks was observed. The near-field fluorescence image of the InGaN microdisks with sun-like e-beam resist structure demonstrates the possibility of using gratings made along the circumference to achieve high directional emission.

A. Experiments

The conventional optical far-field images of the microdisks, which are digitized by using a CCD in connection to an Olympus BX microscope, are compared with the near-field light emission of these microdisks. Near-field optical imaging measurements were carried

out on a commercial NSOM-100 from RHK/Nanonics company (Fig.6). The scanner has the scan range of 30μm in x-, y-, and z-direction. Combined with an optical microscope (Olympus IX70), it is convenient to select the area of interest to observe in the case of micro-device imaging. The fiber probe was an Al coated monomode fiber at 630nm, provided by Nanonics. The length of the cantilevered tip is about 400μm. Optical signals from fiber tip are sent to a sensitive avalanche photon counting module with a dark count of less than 100s^{-1}. The optical signal can also be sent to an SPEX 340 spectrometer through the fiber probe for near-field spectroscopy, the scattered light is collected by a CCD array (300×1100 pixels) located at the end of the spectrometer. Reflection mode schematic and transmission mode schematic were used for InGaP/InGaAlP system and GaN/InGaN system separately.

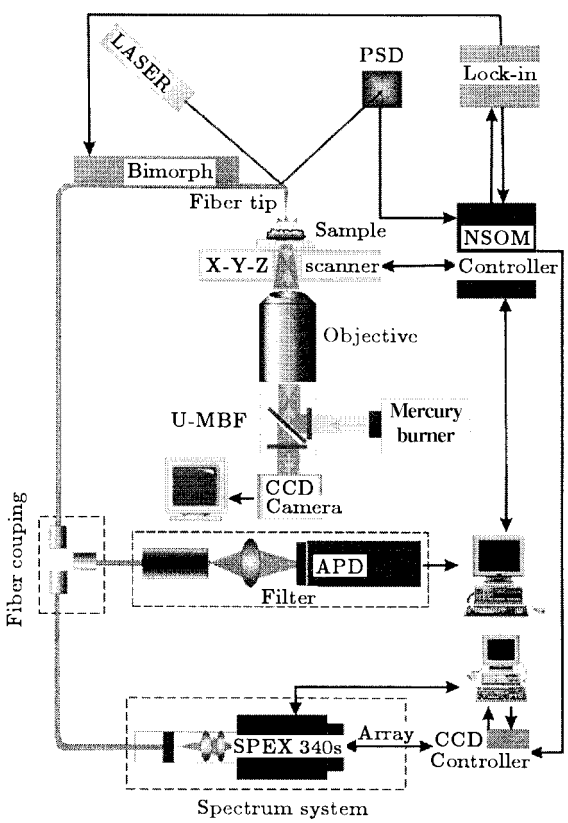


Fig.6. A schematic of the near-field optical imaging and near-field spectroscopy experiment. A photon counter (APD) detects the optical signal collected by cantilevered fiber tip.

The semiconductor InGaP thumbtack-like microdisks were fabricated by using liquid phase epitaxy (LPE) technique and the subsequent micro-fabrication processing.[11] The InGaP microdisks were made with radii ranging from 3–5μm, the thickness about 0.15–0.2μm with a rhombus shaped support column and the height of 1–2μm. It has a shape as a micro-desk sitting on the wafer of GaAs.

The wafers used to prepare InGaAlP microdisks were epitaxially grown by low-pressure metal-organic chemical vapor deposition (LP-MOCVD). The InGaAlP quantum well (QW) circular cylindrical and deformed microdisks with radii about 2.5 to 10μm were prepared by electron beam lithography and wet etching processing etc.

These two types of microdisk are both based on GaAs substrates. A solid frequency-doubled diode laser at wavelength of 532nm was used to excite the PL for these types of microdisks. The emission wavelength is about 620nm to 670nm.

The GaN microdisk were made by epitaxial growth of GaN on sapphire substrate using low pressure MOVPD and followed by a patterning process. The radii of GaN microdisks are ranging from 5–8μm, the thickness is 0.5–2μm.

The InGaN multi-quantum-well microdisk with sun-like E-beam resist structure has the most complicated geometrical structure among microdisks we fabricated. InGaN multi-quantum-wells were grown by means of MOVPD and consisted of four cycles of $In_{0.06}Ga_{0.94}N/In_{0.22}Ga_{0.78}N$ plus one layer of $In_{0.06}Ga_{0.94}N$ at the end. The thickness of $In_{0.06}Ga_{0.94}N$ and $In_{0.22}Ga_{0.78}N$ are 10nm and 2nm, respectively. The radii of InGaN microdisks are 5.6μm. There is a GaN overlayer with thickness of 2.5μm between the InGaN multi- quantum-well and the sapphire substrate. The GaN overlayer was also made a disk-like shape except the sidewall was a little oblique due to the microfabrication processing. Some e-beam resist strips are made along the circumference of the disk and some rings on the top surface.

We used the 330–385nm band in a mercury lamp to excite the PL for GaN and InGaN microdisks. The mean PL peak of GaN microdisks at room temperature and 77K is 552nm. The PL peak of InGaN microdisks is centered at 430nm

B. Results and discussion

1. InGaP/InGaAlP system

Whispering-gallery mode can be observed clearly by the far-field fluorescence images of the InGaP thumbtack-like microdisk. Both excitation and collection are in vertical direction. Figure 7(b) was taken

at room temperature. A bright and narrow red fluorescent ring can been seen clearly along the edge of the microdisk.

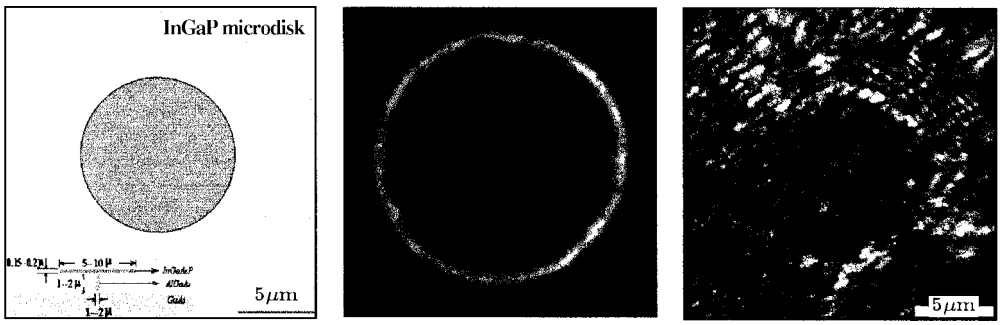


Fig.7. (a) Schematic of the InGaP microdisk, the structure and dimensions are shown in the lower inset. (b) Far-field fluorescence image of InGaP microdisk with a diameter of 10μm. Measured at room temperature, magnified by a 100× objective lens. (c) Near-field fluorescent mapping of InGaP microdisk with a diameter of 10μm, the disk is located at the center. The fluorescent wavelength is 650nm and the excitation wavelength is 532nm.

The near-field fluorescent images were acquired at constant height mode, since the constant tip-sample separation method in contact mode might destroy the delicate microdisk structure and introduce unwanted optical error signal. Figure 7(c) shows the fluorescent light distribution above the InGaP microdisk at a constant height of one wavelength. Much more features are showing in the SNOM images of the microdisk. The bright spots along the circumference of disk unevenly distributed close to the disk edge. We also observed concentric patterns of light both inside and outside the disk. The periods of the concentric rings are about 250nm inside and 500nm outside of the disk, respectively.

Due to uncontrollable directionality, it actually is a big problem to apply WGM mode microdisks in the applications of microdisk lasers. To get directional emission from microdisk should be one of the important projects on microdisk. In particular, recently Gmachl etc. of Bell Labs and Yale scientists[12,13] on the base of microdisk achieved a dramatic result. The directionality and power output were substantially improved by imposing a flattened quadrupolar deformation onto semiconductor microdisk lasers emitting at wavelength of mid-infrared 5μm in temperature range from 40–100K. As they emphasized, the approach is applicable to other semiconductor micro-cavities at visible and near-infrared wavelength. Among various types of semiconductor micro-cavity, the microdisks emitting at visible wavelength is very interesting. We designed and fabricated the circular and deformed mesa-like microdisks patterns. In the cylindrical coordinate, the boundary of the deformed disk is described by the equation of $\rho(\phi) = \rho_0[1+2\varepsilon\cos(2\phi)]^{1/2}$, which was same as Gmachl's experiment. Where $\rho(\phi)$ is the distance between original point to a point on the boundary, ϕ is the angle respect to the axis, ρ_0 is a constant, while ε is the deformation parameter. When ε=0, the disk is a circular disk in shape. When ε is smaller than 0.15, it looks like an approximate ellipse, while ε is around 0.15–0.20, it looks like an "flattened" quadrupolar or a stadium. For different ε but a fixed ρ_0, the total area of the disk is the same. In our experiments, ρ_0 was chosen from 3–10μm and ε was varied from 0 to about 0.2.

The preferential emission in InGaAlP quantum well (QW) circular cylindrical and deformed microdisks was visually observed from the far field(Fig.8). When the cross section of microdisk was gradually deformed from circle, the change of fluorescence image from uniform ring towards 2 or 4 favorable emission along the circumference of microdisks was confirmed. The deformation could be caused by either the shape or etching profile of the disk waveguide.

Concentric patterns of light distribution both inside and outside the disk was observed in the near field fluorescence mapping images as well (Fig.8b). But the periods of the concentric rings are about 1000nm outside of the disk. No obviously emission directionality enhancement can be observed in near field. More detailed investigation such as optimizing QW structure and technique procedure as well as disk mode measurement and analysis are in progress.

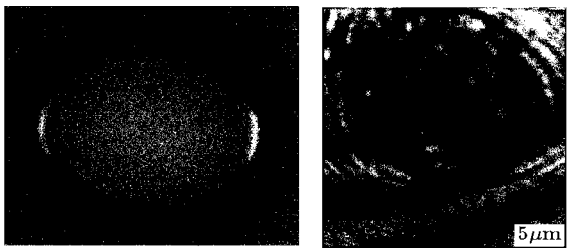


Fig.8. (a) Far-field fluorescence image of InGaAlP microdisk with a deformed parameter ε=0.14; (b) Near-field fluorescent mapping of InGaAlP microdisk with a diameter of 10μm, the disk is located at the center. The fluorescent wavelength is 620–670nm and the excitation wavelength is 532nm.

2. GaN/InGaN system

We also fabricated WGM optical microdisks in GaN/InGaN system. WGM can be observed clearly in these disks as well, both in far field and in near field. In contrast to the case of InGaP/InGaAlP disks, we did not observe the fringe pattern both inside and outside the GaN disk. These discrepancies can be interpreted as the difference in the structure and optical confinement.

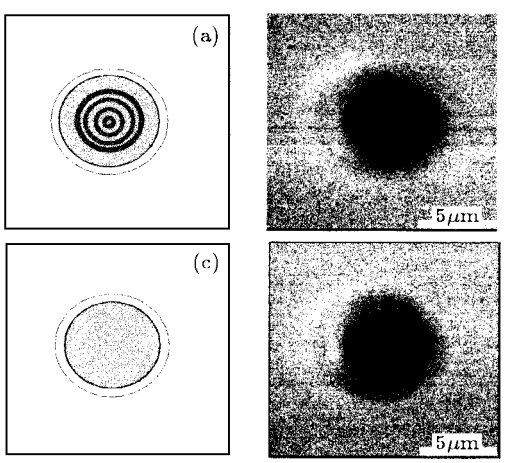


Fig.9. Schematic of disks with e-beam resist rings (a) and without e-beam rings (c); Near-field mappings: (b) for disk (a) and (d) for disk (c)

To control both direction and intensity of light output, Levi *et al* had made gratings or small indentations on the circumference of the disk.[13] Different from the cases above, in which radius of curvature is changed at the disk edge, we fabricated some e-beam resist microstructures with refractive index different from the active material (InGaN) along the circumference or on the top surface of the microdisk in order to achieve directional emission.

We mapped the fluorescence of two types InGaN microdisks (Figure 9(a)(c)) in near-field. Figure 9(a) and (b) give the schematic and the near-field mapping of the disk with only some e-beam rings on the top surface, while 9(c) and (d) shows that of a disk without E-beam resist structure at all. The two fluorescence images are very similar. Both of them show two bright rings, one is along the disk edge while the other outside the disk.

Figure 10 shows the schematic of the microdisk structure and the near-field fluorescence images acquired under constant height mode with the distance between tip and disk surface less than 400nm. From Figure 10(b), one can observe some bright spots evenly located along the circumference of the microdisk, the number of the spots is the same as that of the e-beam resist strips. Some bright strips can also been seen clearly outside the disk edge.

We believe the bright spots and strips in Figure. 10(b) are caused by the e-beam resist strips along the disk edge, since these e-beam resist strips act as waveguide which can guide the whispering gallery mode (WGM) outside from the circumference of the microdisk. However, compared Figure 10(b) and Figure 9(b) with Figure 9(d), the effect of waveguide is not be observed on the top surface of the disk, although there are also some e-beam resist microstructures on the upper surface. The reason for this phenomenon is that the intensity of WGM is concentrated along the circumference of the microdisk, hence, it is not easy to guide the intensity from the top surface but from the edge of the disk. The two bright rings in Figure 9 (b) and (d) may be caused by the refractive indices of InGaN multi-quantum well and GaN overlayer (n=2.65 for InGaN, n=2.7 for GaN). Instead, the light emitted from InGaN will propagate into GaN layer and confined between surfaces of InGaN and sapphire substrate. Therefore, the bright ring with smaller diameter in Figure 9(b) or (d) corresponds to the light comes from the edge of InGaN microdisk, while the other one with larger diameter comes from the lower edge of GaN overlayer since the shape of GaN overlayer is like a frustum of a cone.

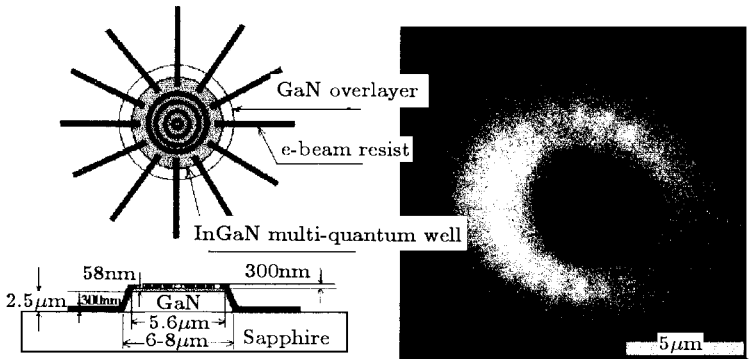


Fig.10. (a) schematic of InGaN microdisk; (b) fluorescent mapping of the disk.

IV. NEAR-FIELD OPTICAL STUDY OF BIO-MOLECULAR (HeLa CELLS)[14]

HeLa cell is defined as any of the cells of the first continuously cultured human carcinoma strain, originally obtained from cancerous cervical tissue and maintained for use in studying cellular processes. Apoptosis is programmed cell death as signalled by the nuclei in normally functioning human and animal cells when age or state of cell health and condition dictates. Cancerous cells are unable to experience the normal cell transduction or apoptosis-driven natural cell death process. The process of apoptos is can be induced by physical factors, such as UV and X-ray, and chemical and biological factors. Its mechanism is not fully understood until now although some significant progresses have been made by scientists. To monitor the apoptosis process is a complex way by characterizing the features of morphology and bio-chemistry, including scanning electron microscopy (SEM), DNA assay, comet assay, and TUNEL (terminal deoxynucleotidyl transferase(TdT)-mediated dUTP nick end labeling), etc. The study on the changes of surface morphology and inner structure and optical properties in apoptosis cell is helpful to build up the apoptosis mechanism. The absorption properties of light of HeLa cells by analyzing their simultaneous normal atomic force (AFM) and near-filed optical images as well as current imaging tunneling spectroscopy (CITS), will be provide some information about the complex process.

A. Sample preparation and experimental procedure

HeLa cells sample covered on a slide were maintained in high glucose Dulbecco's modified Eagle's medium (Gibilco) supplemented with 10% newborn calf serum, 10mM glutamine, and 100 units/ml each of streptomycin and penicillin in a humidified incubator at 5% CO_2.

Induction and assay of apoptosis in HeLa cells were maintained in serum-free DMEM-F12 for 24h prior to experiments. Insulin (5μg/ml) and transferrin (5μg/ml) was added in culture media before C2-ceramide, Hydroxy-ceramide and nonhydroxy-ceramide were diluted into serum-free DMEM at the indicated concentrations. The final concentration of ethanol did not exceed 0.25%. Cell viability was determined using trypan blue exclusion. Blue excluding cells were scored as apoptotic or normal based on morphological criteria: small, round, condensed cells were scored as apoptotic, and all other cells were scored as healthy. For each sample, about 300 cells were scored in a blinded manner, and the experiments were repeated three times.

The RHK/Nanonics SNOM system (Fig.6) ran at tapping mode and transmission- collection mode. Light from mercury burner reflected by a U-MBF filter, then visible light with wavelengths of 404nm, 435nm, 546nm and 577nm was focused onto HeLa sample by a 10x objective (NA=0.30). The transmitted light was collected 20nm a top of the surface by an Al coated tip of 100nm diameter and was fed either to an avalanche photon counter (APD)(SPCM-AQR-14 from EG&G) with a dark count of less than 100 photon/s or a spectrometer (SPEX340S). In order to study the effect of light with different wavelength on the optical image, a band pass filter (500nm to 600nm) was placed in the front of the APD. The spectrum was measured by a 2-dimensional CCD spectrometric detector from Prinston Instruments, TE/CCD-1100P, with the quantum efficiency of 80% @600nm. The surface morphology (AFM imaging) and optical transmission image (SNOM image) and spectroscopy

can be obtained simultaneously.

The CITS was performed over 128×128 pixels. When the tip moved to one pixel, it was standing there, the feedback controller of SNOM sent 5V TTL signal to ignite the spectrometer to collect the spectrum signal from the fiber tip. After 10s collection, the tip continued to move to next pixel.

In order to get distinct image, the feedback system of SNOM should be adjusted to optimum. The scan rate of each line was about 7s. Micrographs from scanning electron microscopy were used to compare with the atomic force images from SNOM.

B. Results and discussion

It is worthwhile to compare the difference of surface morphology from SEM and SNOM. A SEM picture in Fig.11(a) shows small apoptosis cells and many fine dentations. Some rods with size of 100nm-200nm are seen clearly. The thickness of the cell is about 2.5μm, the size is about 15μm×15μm.

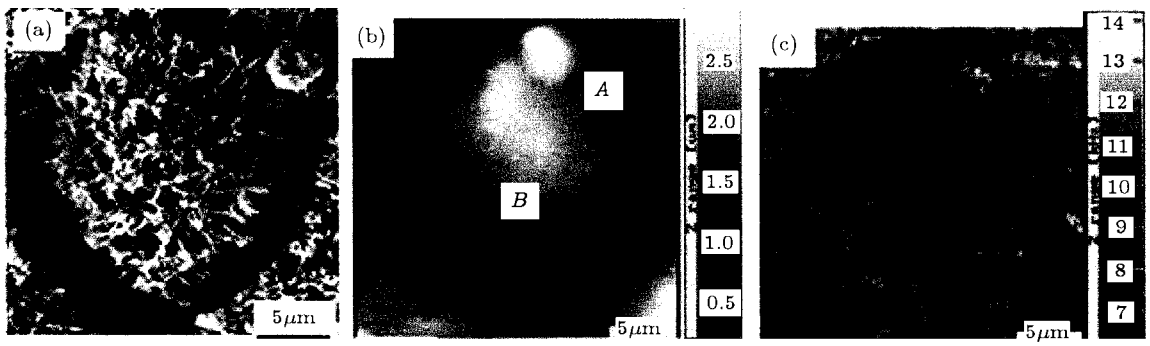


Fig.11. The surface morphology of HeLa sample from SEM (a), simultaneously AFM (b) and near-field images (c) by SNOM

Figure 11(b) shows the topography of the cell (AFM), it does not show more details than that in Fig.11(a), where the height of the cell is about 2.95μm, the size is about 15μm×15μm. Some apoptosis small cells with the size of 500nm–4μm and with the height of 50nm to 400nm cover the big cell. The resolution of our SNOM system is decided by the diameter of the fiber tip, which is about 100nm in our case, hence, the resolution of our SNOM is less than that of SEM. Besides, the interaction between the tip and the sample will broaden the features on the surface of sample.

However, SEM picture can only give the information over the surface of HeLa cell. What is more attractive for biologist is what is happening in the internal structure of cell. As we know, only SNOM has the ability to satisfy this request.[3] The near-field optical image is able to bring more information about the inner details of cell by measuring the variation of transmitted light intensity through the sample. Figure 11(c) was simultaneously captured near-field optical image with Fig.11(b). It has detailed contrast changes that are not seen in AFM image (Fig.11(b)). Small, round, condensed cells are apparently observed in Fig.11(c). The distribution of light over the HeLa cell are inhomogeneous. This proofs that the inner structure of the cell aggregated together inhomogenously. We analyses the properties of two special regions marked "A" and "B". The height in position "A" is about 2.2μm, higher than that in Region "B" of 1.5μm. Fig.11(c) shows that the photon count in "A" is 13,000 photon/s , count in "B" is 7500 photon/s, where the heights at two positions are alike. The component in region "A" may have a function to enhance light transmission. This is as if some microstructure in the cell in this region is concentrating the light in certain biological structures that act as optical waveguide which has been observed in literature.[3]

For studying the inner structure of cell, CITS is a powerful method by measurement the variation of the integral intensity of spectrum. Figure 12(a) is the contour profile of surface morphology (Fig.12(b)). Figure 12(c–f) show the intensity variation of transmitted light with the wavelength of the illumination of the light and the thickness of cell. When the wavelength changing from 404nm to 434nm, the absorption area in the center part of the cell was enlarged. Then the absorption area broke into two parts at 546nm and 577nm. This indicates some structure in the internal cell is more transparent at longer wavelength light.

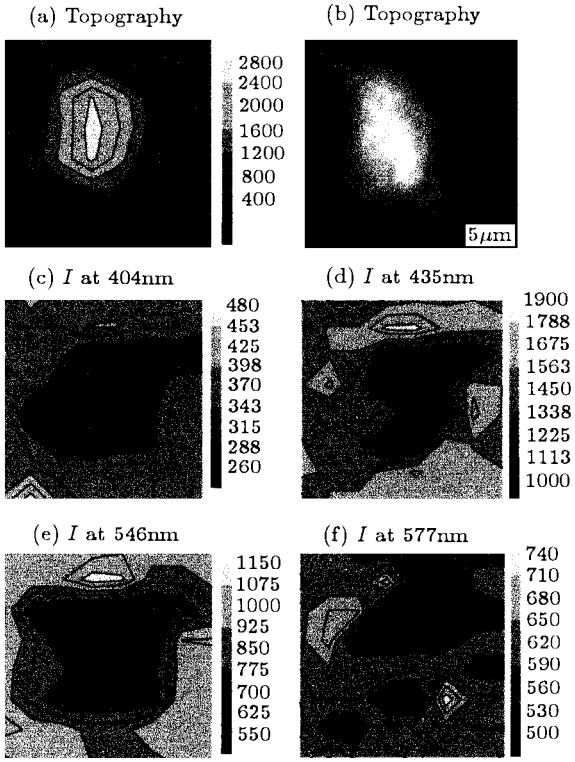


Fig.12. The dependence of the intensity of transmitted light on the wavelength and thickness of the HeLa cell. Image area was $25\mu m \times 25\mu m$.

Another area was chosen to study the effect of inner structures. Figure 13(a) and (c) are the simultaneous AFM and near-field images over the area illuminated by mercury light containing four lines of 404nm, 435nm, 546nm, 577nm. Inserting a band pass filter (from 500–600nm) in the front of APD, the simultaneous AFM and near-field images over the same area are shown in Fig 13(b) and (d). The AFM images are similar as expected. There exists some remarkable difference in optical images Fig.13(c) and (d). The profiles of one cross section labelled line AB in Fig.13 show in Fig.14(a) and (b). The surface morphology in Fig.14(a) is of consistency. The intensity of transmission light (Fig.14(b)) is nearly similar except for the region of $2\mu m$–$6\mu m$. There appears a strong absorption to green light (546nm and 577nm).

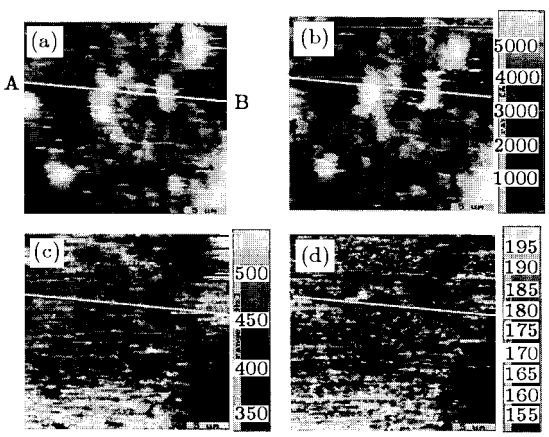


Fig.13. The simultaneously AFM (a) and (b), near-field images (c) without the band pass filter and near-field images (d) with the band pass filter (500nm-600nm).

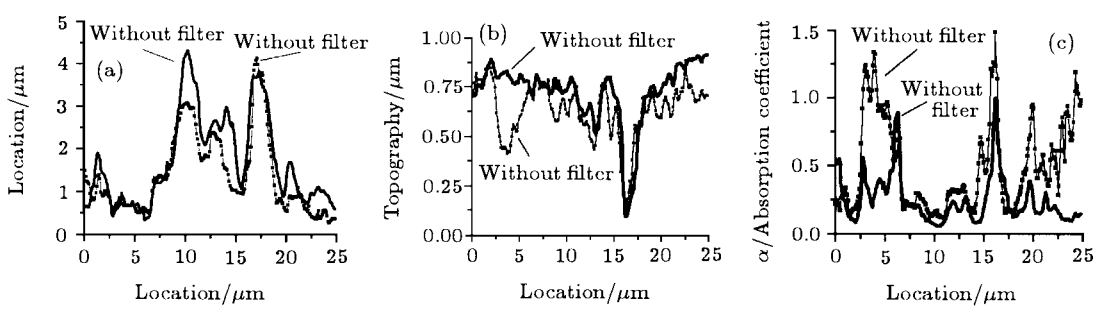


Fig.14. The profiles of AFM image (a) and intensity of transmission light (b) , the absorption coefficient of the section marked line AB in Fig.13.

The absorption coefficient α of the cell, induced from variation of intensity based on Bouguer-Lambert Law, $I = I_0\ e^{-\alpha z}$, where I_0 and I are the intensities of the light at the entrance to and exit from a cell of thickness z, is shown in Fig.14(c). At the region of $2\mu m$–$6\mu m$, α with the filter is three times larger than that without the filter. In this region, the cell should be opaque to green light, which is contrary to phenomena in Fig.12(e) and (f), where it seems to be little more transparent to green light. From this point, we can induce that the cells in Fig.12(b) and at the region of $2\mu m$-$6\mu m$ in Fig.13 (b) were in different apoptosis status. The changes in the inner structure, such as the size, concentration and density of dense bodies and the aggregation of chromatin, have a different function on the light transmission. Meanwhile, α is dependent on

the variation of thickness of the cells. The results are definitely not due to the topography variations. It indicates that the process of apoptosis of HeLa cell is much more complex. Further to understand the complicate process of apoptosis, other experiments, such as tracing the evolution of the cell through the detection the fluorescent features of the dyed HeLa cells, will be carried out in our group and are expected to give more evidence to reveal the apoptosis mechanism.

V. SUMMARY

We have designed a low temperature SNOM system. This system is suited for both nanometer scale imaging and spectroscopic application. The resolution of shear force imaging were about 100nm. A special designed coaxial double lens was used to introduce the illumination beam through a 200μm fiber; the detected optical signal was transmitted via a fiber tip to an avalanche photon detector.

By using scanning near-field optical microscopy technique at room temperature and atmosphere, we have studied the fluorescent light distribution of InGaP/InGaAlP and GaN/InGaN semiconductor microdisks in the near-field. Whispering gallery mode has been observed at the top surface of these microdisks by using near-field optical method. The light distributions of them are quite different due to the different disk structures and optical confinements. Both ring-like emission intensity along the circumference of the disk and an even intensity distribution inside the disk are observed. This can be interpreted as the combination of the WGM with Fabry-Perot mode. Due to the waveguide effect of e-beam resist structure, light emissions from certain directions are enhanced which can be seen from the bright spots and strips in the near-field fluorescence image.

We have obtained topographic (AFM) and near-filed optical image as well as CITS mapping of apoptosis HeLa cells by SNOM, which is operated at transmission-collection mode and tapping mode. Compared to SEM and AFM images, the near-field optical image showed considerable contrast in HeLa cells, and provided more details about the apoptosis features. The inner structure of the cell aggregated together inhomogenously, resulting in the different transmission ability to the illuminating light with different wavelengths light at different stage of apoptosis. The complicated apoptosis process would be revealed if we trace the evolution of the cell through the detection the fluorescent features of the dyed HeLa cell. This work is being performed in our laboratory.

ACKNOWLEDGMENT

The work was supported by National Natural Science Foundation of China under Grant Nos. 19890380, 10074002, 30070388 and by The Research Fund for the Doctoral Program of Higher Education and SRF for ROCS, Ministry of Education, China

References

[1] Hecht B, Sick B, Wild U P, Deckert V, Zenobi R, Olivier J F, Dieter M and Pohl D W 2000 *J. Chem. Phys.* **112** 7761

[2] Dunn R C 1999 *Chem. Rev.* **99** 2891

[3] Meixner A J and Kneppe H 1998 *Cellular and Molecular Biology* **44** 673

[4] Zhu X, Fei T, Yin Y, Xu S F, Zhou H T and Gan Z Z 2000 *Near-Field Optics: Principle and Applications* (World Scientific) **150**

[5] Karrai K and Grober R D 1995 *Appl. Phys. Lett.* **66** 1842

[6] Ghaemi H, Cates C and Goldberg B B 1995 *Ultramicroscopy* **57** 165

[7] Zhu X, Shen Y M, Zhang Y, Xu S F, Dai L, Chen Y Q, Feng W, Wang D J, Xing Y C, wang G Z, Zhang B, Zhou H T, Zhang G Y and Gan Z Z 2000 *Near-Field Optics: Principle and Applications* (World Scientific) **263**

[8] Fratechi N C and Levi A F J 1995 *J. Appl. Phys.* **80** 644

[9] McCall L, Levi A F J, Slusher R E, Pearton S J and Logan R A 1991 *Appl. Phys. Lett.* **60** 289

[10] Zhu X, Zhang Y, Xin Y, Dai L, Wang R, Zhang B, Ling Y, Zhou H, Wang G, Yin Y, Zhang G and Gan Z 1999 *J. of Microscopy* **194** 439

[11] Zhu X, Zhang Y, Xin Y C, Ling Y, Wu K, Zhou H T, Yin Y, Zhang B and Gan Z Z 1998 *Proceedings of SPIE* **3467** 231

[12] Gmachl C, Capasso F, Narimanov E E, Nockel J U, Stone A D, Faist J, Sivco D and Cho A 1998 *Science* **280** 1556

[13] Levi A F J, Slusher R E, McCall S L, Glass J L, Pearton S J and Logan R A 1993 *Appl. Phys. Lett.* **62** 561

[14] Xu S F, Shen Y M, Liu X L, Hu J C, Lu P, Zhou H T, Zhai Z H and Zhu X 2000 *Accepted by Solid Charaterization* **7**